Ocean Sci. Discuss., 9, 1387–1436, 2012
www.ocean-sci-discuss.net/9/1387/2012/
doi:10.5194/osd-9-1387-2012

Ocean Science Discussions

Observed response of the marine atmospheric boundary layer to the Southern Ocean fronts during the IPY BGH 2008 cruise

C. Messager[1], **S. Speich**[1], **and E. Key**[2]

[1]Laboratoire de Physique des Océans, CNRS/INSU, UMR6523, BP 70, 29280 Plouzané Cedex, France
[2]National Science Foundation, Office of Polar Programs, 4201 Wilson Blvd, Arlington, VA 22230, USA

Received: 8 March 2012 – Accepted: 12 March 2012 – Published: 28 March 2012

Correspondence to: C. Messager (christophe.messager@ifremer.fr)

Published by Copernicus Publications on behalf of the European Geosciences Union.

Abstract

A set of meteorological instruments was added to an oceanographic cruise crossing the Southern Ocean from Cape Town to 57°33′ S on board the R/V *Marion Dufresne* during the summer 2008. The Cape Cauldron, the subtropical, subantarctic, polar and southern Antarctic circumpolar current fronts were successively crossed. The recorded data permitted to derive the exchange of momentum, heat and water vapour at the ocean-atmosphere interface. A set of 38 radiosonde releases complemented the dataset. The marine atmospheric boundary layer characteristics and air-sea interaction when ship crossed the fronts and eddies are discussed.

The specific role of the atmospheric synoptic systems advection on the air-sea interaction is highlighted over these regions. The dynamic associated with these systems drive the vertical mixing of the MABL by wind shear effect and/or the vertical thermal mixing. The MABL is stabilized (destabilized) and mixing is inhibited (enhanced) over the warm front sides if meridional wind component is northerly (southerly).

1 Introduction

Several in-situ observational studies have previously identified some interactions between the Sea Surface Temperature (SST) and the atmosphere over regions where intensive and highly variable mesoscales activity is persistent: Gulf Stream, Kuroshio and Agulhas currents (Businger and Shaw, 1984; Jury and Walker, 1988; Friehe et al., 1991; Rouault and Lee-Thorp, 1996; Kwon et al., 1998; Giordani et al., 1998; Rouault and Lutjeharms, 2000; Rouault et al., 2000; Bourras et al., 2004, Tokinaga et al., 2006). All these papers described the SST fronts interaction with the atmosphere and the wind changes near the surface and throughout of the Marine Atmospheric Boundary Layer (MABL). The past decade of satellite observations permitted to generalize the relationship between SST and surface winds at oceanic mesoscales over many regions. The

OSD
9, 1387–1436, 2012

review of these interactions, in-situ, remotely and numerically identified, can be found in Chelton et al. (2004), Xie (2004) and Small et al. (2008).

The interactions were mainly investigated in the Northern Hemisphere western boundary current systems (e.g. Kwon et al., 2010; Kelly et al., 2010) and less is known on the Southern Ocean (SO) frontal systems and its effect on the atmosphere. The main feature of the SO is its conspicuous frontal banding (i.e. Orsi et al., 1995; Belkin and Gordon, 1996). The SO is limited to the north by the Southern Subtropical Front (S-STF), which separates subtropical and subantarctic waters. South of it flows the Antarctic Circumpolar Current (ACC) which consists of multiple branches and filaments that are gathered to represent the main ACC fronts (Swart et al., 2008; Sokolov and Rintoul, 2009a, b). The fronts often exhibit considerable latitudinal variability on their circumpolar path. These forms of variability are dominant in the meso scale induced by front meandering and eddy genesis (Lutjeharms and Valentine, 1988; Stammer, 1998; Phillips and Rintoul, 2000; Morrow et al., 2004).

The S-STF also marks the southern limit of the Agulhas current which transports warm water along the south-east coast of Africa and which is regarded as the strongest western boundary current in the Southern Hemisphere and the largest in the world ocean (Bryden et al., 2005). South of Africa, its retroflexion, the Agulhas Retroflection, has a large impact on climate, regional weather and marine ecosystem (Lutjeharms, 2006). This powerful current produces meanders, which eject many persistent eddies (Lutjeharms and van Ballegooyen, 1988; Boebel et al., 2003). Eddies, fronts, and filaments associated with the Agulhas Current and Retroflexion are spatially extensive with sharp horizontal SST gradients. These surface discontinuities impact the air-sea exchanges locally and regionally (Jury and Walker, 1988; Lee-Thorp et al., 1999; Rouault and Lutjeharms, 2000; Reason, 2001; Small et al., 2008).

The hydrographic structure and frontal systems between Africa and Antarctica have been studied and described (e.g. Lutjeharms and Valentine, 1984; Belkin and Gordon, 1996; Swart et al., 2008; Gladyshev et al., 2008) but little work were conducted to better understand the regional and temporal variability of the SO fronts south of

OSD
9, 1387–1436, 2012

Africa (Sokolov and Rintoul, 2009a; Swart and Speich, 2010). Evermore, the specific issues related to the SO south of Africa versus atmospheric dynamics were poorly documented. However, within the Agulhas Current system, north of the S-STF, the response of the MABL to a SST gradient has been already described by Walker and De Mey (1988), De Mey et al. (1990) or Rouault et al. (1999). A more spatially extended study (Rouault and Lee Thorp, 1996) described measurements of the MABL between Cape Town and Marion Island. However, no atmospheric campaign crossed successively the Cape Basin, the S-STF (covering the western subtropical convergence windward the Agulhas Retroflection area), and all the ACC fronts. This latter region has thus a poor set of ocean-atmosphere measurements compared to other regions over the world, despite its importance for the climate and the global warm exchanges between the Indian and the Atlantic oceans as well as with the atmosphere (Lutjeharms, 2006).

The international GoodHope program was undertaken in 2004 to monitor the exchange of water and properties between the Atlantic and Indian oceans, and to better understand the processes involved in these exchanges (e.g. Ansorge et al., 2004). The 2008 cruise of the GoodHope program was carried out in the framework of the International Polar Year, and was named the BONUS-GoodHope cruise (hereafter BGH), as it associated the fourth hydrographic sampling of the GoodHope line with atmospheric and biogeochemical measurements constitutive of the BONUS program. The BGH cruise followed the track presented in Fig. 1 and crossed successively the Cape Basin, the STF and the ACC fronts. Starting from Cape Town in South Africa (13 February 2008), the R/V *Marion Dufresne* sailed south-westwards to reach the Greenwich line, on which it sailed south until 57°33′ S (18 March 2008). The BGH cruise was an opportunity to deploy some atmospheric measurements over these regions where in-situ data are rare due to severe weather conditions (much of the regional history has been derived from satellite retrievals). It was the first time this section was instrumented with atmospheric measurements in order to have continuous surface information as well as vertical structure of the MABL through the regular releases of radiosondes (see

OSD
9, 1387–1436, 2012

Sect. 3). These measurements also allowed the computation of surface fluxes. A large set of meteorological data was continuously sampled in order to analyze changes in the atmosphere close to the surface while crossing remarkable ocean features (fronts, eddies).

The aim of this paper is thus to present the set of atmospheric observations performed during the BGH cruise. Moreover, the specific role of the atmospheric synoptic system advection on the air-sea interaction over SST anomalies (fronts and eddy) is highlighted as well as the vertical mixing of the atmospheric boundary layer.

2 Ocean dynamics and fronts

The BGH route was planned to maximize sampling of the complex oceanic temperature fields, which included short-lived filaments, mesoscale eddies, and SO fronts. The regional upper-ocean structure together with the frontal locations is shown in Fig. 1, where fronts are drawn using satellite altimetry (Swart and Speich, 2010; Arhan et al., 2011), and Argo float data (Faure et al., 2011). However, their precise locations evocated hereafter are determined using the hydrographic data collected during the survey and classical hydrographic criteria (e.g. Orsi et al., 1995; Belkin and Gordon, 1996) (see also Fig. 2).

Compared with Drake Passage and south of Australia, the oceanic sector south of Africa constitutes the most dynamic and variable of the SO. The Agulhas Current, which lies along the south-eastern edge of the African continental shelf, is marked by a region of extreme mesoscale variability (Lutjeharms, 2006) in the form of eddy shedding that is associated with the current retroflecting back toward the east (Gordon, 1985; Duncombe-Rae, 1991; Lutjeharms, 1996; de Ruijter et al., 1999; Boebel et al., 2003). The Agulhas Retroflection region is characterized by an intermittent stream of anticyclones (Agulhas Rings) and cyclones (Lutjeharms and Gordon, 1987; de Ruijter et al., 1999). The rings are occluded from the Agulhas Retroflection, propagate generally in

OSD
9, 1387–1436, 2012

a north-westward direction (Schouten et al., 2000), then intersect the GoodHope line in the subtropical domain (Gladyshev et al., 2008; Swart et al., 2008).

The ACC is characterized by a series of eastward jets associated with baroclinic fronts, which denote the positions of the maximum meridional thermohaline gradients (e.g. Orsi et al., 1995; Belkin and Gordon, 1996). In the African sector of the SO, four primary fronts exist: the Southern Subtropical Front (S-STF), the Subantarctic Front (SAF), the Polar Front (PF), and the southern ACC front (SACCF). Additionally, the southern boundary of the ACC (SBdy) marks the limit separating flow between the ACC and Weddell Gyre system (Orsi et al., 1993). The spatial structure of the S-STF south of Africa is complicated by the presence of Agulhas Rings, particularly in the region of the BGH line, in the Cape Basin. At this location, the presence of the S-STF is made up by an almost continual "stream" of eddies (Lutjeharms and Valentine, 1988; Belkin and Gordon, 1996; Dencausse et al., 2010). Because of this complex subtropical-subantarctic transition south of Africa, the detection of the S-STF led to a wide latitudinal span, from 38°20′ S to 42°′ S, suggestive of two branches at these latitudes during the BGH cruise. The northern limit of this interval shows the most pronounced gradient (e.g. a SST drop of 5 °C and salinity change from 34.7 to 35.0, at 100 m), and lies at the southern border of the wide saline domain ($S > 35.0$) marking the border of an Agulhas ring (Arhan et al., 2011). The northern branch of the S-STF was crossed on 24 February (day 55 since 1 January 2008). The southern limit of the S-STF coincides with the southern border of an Agulhas cyclone that was shed 4.5 months before from the Agulhas Banc (Arhan et al., 2011). This cyclone – so-called "S eddy" – was crossed the 26 February (day 57) from 40.6° S to 42.5° S while one of the southern variety of Agulhas Rings – so called "M-eddy" – was crossed just north of the SAF, from 42.7° S to 44° S, during the 28 and 29 February (days 59 and 60). This latter ring was 9.5 months old.

The SAF was located at 44.17° S and crossed during the 28 and 29 February (day 59 and 60). Following Orsi et al. (1995) the PF was located at the northern end of the domain where a shallow (<200 m) vertical temperature minimum can be found

OSD
9, 1387–1436, 2012

at 50°22′ S. The PF was thus crossed the 8 March (day 68). The Southern ACC Front (SACCF) location (52°56′ S) was crossed the 12 March (day 72). The Southern Boundary of the ACC (SBdy) was found at 55°54′ S and crossed on March 14 (day 74). The last BGH station was carried out at 57°33′ S south of the ACC, in the Weddel Gyre the 16 March.

3 Instruments and data

A total of 111 hydrographic profiles were obtained at 79 geographical stations, from the African continental slope to beyond the ACC Southern Boundary along the Greenwich meridian. Further information on the various measurements may be found in the cruise report (Speich and Dehairs, 2008), and details of the hydrographic measurements in the Conductivity-Temperature-Depth (CTD) data report (Branellec et al., 2010).

The atmospheric data were collected by classical atmospheric measurements as well as radiometric and radiosounding processes.

The set of instruments was composed by a standard weather station (the Weatherpack) modified for at sea application; an interferometer and a radiosonde station (see Table 1).

Most of the instruments except the radiosonde receiver were installed above the footbridge at 20 m height. Attention was paid to limit the effect of the ship on each instrument, which included profiling and imaging, as well as those which required adequate ventilation and clear lines-of-sight. On the forward railing, to the starboard side of the centreline, two tabs were welded to allow a secure deployment of the Weatherpack and radiation sensors on a T-frame. The Weatherpack provided minute-averaged measurements with a Young anemometer (for wind speed and direction) as well as sensors to measure air temperature, relative humidity and barometric pressure. It was mounted at the top of the "T". The Eppley pyranometer and pyrgeometer dedicated to longwave and shortwave radiations recording (minute-averaged) were placed on gimbals at the end of each arm of the "T". The plates which house the meteorological measurements

OSD
9, 1387–1436, 2012

were well-ventilated to ensure the best quality data. The Eppley domes were maintained daily to remove traces of precipitation and soot from the ship's smokestack. The two gimbals reduced the effect of ship motion, particularly pitch and roll, on the measurements. Dome temperatures were recorded for the pyrgeometer during the cruise and used in post-processing to ensure the highest accuracy longwave measurement.

Along the leg, 38 radiosondes were released providing vertical profiles of the Marine Atmospheric Boundary Layer (MABL) in relation to ocean features. All the radiosondes used were Vaisälä RS92-SGP starting at 14m above sea surface reaching up to between 5000 m and 29 000 m, measuring temperature, humidity, wind speed, wind direction and pressure along a vertical profile following radiosonde ascension. Each sounding was calibrated using a ground-check unit before launch. The soundings were released with preference towards 12:00 UTC and 18:00 UTC. Some were also released irregularly; either at 00:00, 06:00, 12:00 or 18:00 UTC when fronts or eddies were encountered. Additionally, two diurnal cycle measurements were performed during two long stations (cf. Speich and Dehairs, 2008) at a fixed location. The sounding locations and times of release are presented in Table 2. The sampling frequency for all sounding variables was 10s before the 4 March 2008 and one second afterwards.

An interferometer, the M-AERI (Marine-Atmospheric Emitted Radiance Interferometer) which measures infrared spectra between 3–18 µm was sited on the starboard railing, with clear field of views of the sea surface and of the sky overhead. Its measurement cycle includes two blackbody calibration views, as well as views of zenith, and ±55°, which combined takes approximately 10 min to complete. Spectra collected from each view are used to calculate the air temperature and sea surface skin temperature with very high accuracy (deduced from the 7.7 and 14.1 µm channels). During times of snow, spray, or rain, the instrument is taped to protect the sensitive electronics inside and to prevent against degradation of the mirror surface.

Additionally, an automatic meteorological METEO-FRANCE station "BATOS" as well as a Gill sonic anemometers were installed in the main mast of the ship. A second

OSD
9, 1387–1436, 2012

sonic anemometer was installed on the forward mast. A second radiation sensor was installed in the forward ship's mast.

The Sea Bird thermosalinograph bulk temperature was used as the bulk SST measurement at 6 m depth with a sampling rate of 1 min. The CTD data were used to control and calibrate periodically the thermosalinograph.

The surface measurements are presented in Fig. 2 while Figs. 3 and 4 present the potential temperature and relative humidity vertical profiles and, the vertical wind profiles respectively.

At any time during the cruise, one of the onboard's meteorologists kept track of the quality of the data and state of the instruments in real time to ensure valuable measurements throughout the entire cruise. A preliminary quality control was applied to all data on board and a rigorous quality control on the measures has been then applied post-cruise to resolve a number of issues common to shipboard sampling of atmospheric and flux variables (possible instrument failures, superstructure influences, sampling gaps, and rain effects). Moreover, an intercomparison and cross validation of all the data collected onboard, by radiosondes as well as satellite datasets were performed in order to obtain the best dataset along the ship track.

The Weatherpack air temperatures and M-AERI air temperature time series generally agreed in magnitude and timing, even if superstructural heating during low wind/high insolation periods introduced heat plumes into the Weatherpack air temperature data. Turbulent eddies and other flow distortions, such as wind acceleration over the edge of the passerelle and shadowing by the ship's mast, also influenced air temperature and wind. These rapid fluctuations are evident in both air temperature and wind time series for the several sampling units. Correlations were performed between data units to isolate lags and M-AERI air temperature data were used as reference to define heat plume events in the Weatherpack and bias in the BATOS air temperatures.

Bulk sea temperatures from the ship's thermosalinograph had also undergone an intercomparison with XBT and CTD data collected at 6 m depth. Once the validity of

OSD
9, 1387–1436, 2012

the thermosalinograph temperature time series was assured, skin-bulk temperature analyses were undertaken with the M-AERI data.

Radiation measured by the gimbaled Eppleys on the Weatherpack were checked to remove only main mast shadow events (and not cloud signatures) from the data. Comparison with the ship's plate-mounted pyranometer on the second forward mast provided another data control.

Finally, the surface turbulent fluxes of momentum deduced from the in-situ observations were computed using COARE "bulk flux" algorithm (Fairall et al., 2003) and are presented in Fig. 5. The turbulent heat flux (THF) is the sum of the sensible heat flux (SHF) and the latent heat flux (LHF). The in-situ solar radiation and net longwave radiation at the surface are also presented with the net heat flux at the surface.

Note that the cruise started on 13 February but the atmospheric measurements started the 16 February.

4 Ocean fronts and MABL

In many regions, the SST fronts are supposed to interact with the aloft atmosphere through the dynamics effects (spatial wind variability) as well as thermodynamics effects inducing an alteration of the vertical structure of the MABL. Many studies deal with the role of SST perturbations on the MABL and, in 2008, Small et al. performed a detailed review of these papers. They mainly focused on the coupling between surface winds and mesoscales SST perturbations and showed that air-sea interactions are enhanced in the vicinity of oceanic frontal regions because of the air-sea surface differences inducing changes in the vertical structure of the MABL mainly controlled by both pressure gradients and the turbulent mixing of momentum as air flows across a front. The atmospheric vertical potential temperature profiles is expected to be stabilized (or neutrally stabilized) over the cold front side and destabilized over the warm front side. This and substantial changes in turbulent heat fluxes across ocean fronts can give rise to some changes in boundary layer structure and height. In some cases, an Internal

OSD
9, 1387–1436, 2012

Boundary Layer (IBL) is formed as air flows across a front. Moreover, differential heating of the MABL across an ocean front tends to create a pressure gradient force in the direction of the SST gradient. The effect on the MABL is to increase (decrease) the wind stress over warm (cold) water through a modification of the vertical structure of the MABL by turbulent heat fluxes.

For the specific case of the wind magnitude changes above SST discontinuities both in-situ and remote (satellite) measurements were used. For these latter, the interaction was highlighted by averaging surface data over weeks in order to reduce the effects of powerful synoptic weather features variability that can hide less energetic signal due to sea surface discontinuities. Such approach is thus more climatic than related to process investigation. However, the SST-wind interaction was also highlighted with in-situ observation but only when synoptic weather conditions were fair enough (wind not exceeding 15 m s^{-1}, whatever the location of the in-situ campaigns) and thus, when MABL structure was rather affected by the predominant local effect.

Small et al. (2008) actually mentioned that the SST-MABL interaction description is complicated by the passage of synoptic atmospheric features but these latter are expected to play an important role in the setting of the vertical stratification. However, once the MABL vertical structure is considered and investigated, the magnitude and the importance of the MABL diurnal cycle is also questionable. In many earth places, this latter drives the vertical mixing when synoptic conditions are fairs. It is remarkable that the literature does not bring any information about this issue for location south of the South African S-STF. It is thus interesting to try to identify the relative role of local sea surface effect, the synoptic features effect as well as the MABL diurnal cycle effect in the observed sea surface-atmosphere interaction when ship met oceanic fronts.

4.1 The STF

This oceanic front appeared as a strong SST gradient of −4 °C per 100 km (Fig. 2a). The ship crossed the STF between the 23 (day 54) and 24 February (day 55) and the wind speed increased accordingly (+6 m s^{-1}; Fig. 2b). The Fig. 2a, b suggest that the

OSD
9, 1387–1436, 2012

oceanic fronts seems correlated to changes in the low atmospheric dynamics by influencing winds but these changes in the wind magnitude can also be explained by coincident synoptic weather variability. The Fig. 6 indeed presents the synoptic situation in the ECMWF ERA interim reanalysis. A low pressure system located to the northeast of the ship and centred on the Cape Basin deepened on these days. The associated wind speed increase was strengthened by the eastward displacement of a high pressure system, which was located to the south along 43° S. For these reasons, the wind increased uniformly over a larger area than the STF area only (Fig. 6b). The reanalysed synoptic wind increase is less than 6 m s^{-1}. The concomitant role of the local pressure gradient variation across the front (see previous paragraph) is here questionable. Note that the wind stayed mainly south-easterly and advected cold and dry air mass over the front (see R_h on Fig. 2a). It was thus the situation of wind blows from a cold SST to a warm SST with a strong breeze magnitude. This type of circulation and the MABL response to an ocean front in a situation with a strong background wind have been already described by Song et al. (2006) and Spall (2007). The increase of turbulent heat fluxes downwind combined to the wind shear tended to destabilize and mix the BL. A deepening of the BL is thus expected downwind the front (over the warmer SST) due to a change in the momentum balance between upwind and downwind to the front.

Two atmospheric radiosondes were released in the vicinity of the STF the 23 and 24 February (rs1 and rs2 respectively). The rs1 was released north of the STF while the rs2 was released south of the STF. The rs1 and rs2 exhibit a profile of an unstable MABL (Figs. 3 and 4). However, the rs2 boundary layer is not as deep as the rs1 and this latter revealed a shallow unstable internal mixed layer bounded by a cloud layer at 900 hPa with a residual unstable layer aloft, whereas the rs2 profile does not exhibit saturation within the BL. The low-level cloud layer observed for the rs1 profile could be associated with the increase of latent heat flux release (not shown, but the THF increase is significant on Fig. 5 around 16:00 UTC) induced by the cold and dry air advection over warm water. These differences in the MABL height and structure upwind and downwind the STF are in accordance with previous observation over intensive frontal

OSD
9, 1387–1436, 2012

regions as described by Spall (2007) when a cold flows (here northwards) passes a SST front from cold (here located south) side to warm side (here located north). The BGH observation illustrates the expected changes in the MABL profile observed north and south of the STF as previously observed for other oceanic region (Gulf Stream, Kuroshio). That complements previous observation conducted within the Agulhas region, relative to the moisture uptake (Lee-Thorp et al., 1999) and the MABL distortion (Jury and Walker, 1988; De Mey et al., 1990; Jury, 1994) observed leeward the Agulhas retroflexion while the STF observations were conducted windward the Agulhas retroflexion area during the BG cruise.

Note that the rs1 profile was likely not totally mixed at 1621 UTC because of the SST exceeded the air temperature by 2 °C. That induced an upward heat flux (Fig. 5) which destabilized the shallow boundary layer. This is sustained by the air flowed from cold to warm water (Fig. 2a, b shows a surface wind of 10.5 m s^{-1}/from 150° advected cold and dry air from the south). The humidity component straightened the upward heat flux since the incoming flux was dry and arrived over a warm SST region with a high potential evaporation. The evaporation was then enhanced corresponding to an observed LHF increase (not shown).

The rs2 profile has been recorded in a similar synoptic condition (Fig. 6c) and in-situ observed wind (12.5 m s^{-1}/from 128°) but earlier in the diurnal cycle (at 12:00 UTC). As the unstable layer just above the surface is not deep as the one observed for the rs1 profile it is not clear how a diurnal cycle can affect the vertical mixing, even if the joint effects of surface gap (SST fronts) and wind seem to mainly drive the MABL response.

4.2 The SAF

The ship stayed at a fixed location (42.47° S/8.93° E), north of the SAF and the M eddy and south of the S eddy (see Sect. 2) from the 26 February (day 57) at 20:32 UTC to 28 February (day 59) at 10:00. During that period, four radiosondes (from rs8 to rs11-see Table 2) were released. The situation is illustrated in Figs. 7 and 8 with the eastward displacement of a low pressure system. Its northern part arrived over the ship

OSD
9, 1387–1436, 2012

before noon the 27 February. Consequently, there was a significant in-situ wind speed increase as well as a direction change (passing from north-westerly to south-westerly) before noon (Figs. 7a and 8c). The relative humidity and air temperature significantly decreased accordingly with the advection of the Antarctic cold and dry air (southwesterly wind) while during the 26 February, the relative humidity and air temperature were relatively high due to the advection of the subtropical air mass associated with the northerly wind.

During this long station, the air temperature was initially higher than the SST until 14:00 UTC (Fig. 7c) the 27 February (day 58). Due to the advection of warm and humid air from the north, the turbulent heat flux thus remained weak and did not tended to destabilize the MABL. The rs8 profile thus exhibits a stable boundary layer (SBL) on early 27 February (00:00 UTC) also known as a classical nocturnal boundary layer (NBL). However these stable conditions persisted from the 26 February (see profiles rs6 at 12:00 UTC and rs7 at 18:00 UTC). The SBL is thus more a result of the synoptic situation rather than a classical NBL because of the northwesterly flow that enhanced the MABL stratification by advecting warmer air than the SST.

After 00:00 UTC the 27 February, the low pressure system arrived over the ship. The SBL persisted for the rs8 (00:00 UTC) sounding however a mixed layer appeared aloft the stable layer for the rs9 sounding (06:00 UTC). This mixed layer (also known as residual layer – RL) corresponds to a vertical mixing mainly enabled by dynamic mixing (wind shear, see Fig. 4). The LLJ nose reaches indeed more than 20 $m\,s^{-1}$ aloft the SBL, inducing a TKE able to mix the atmosphere at these levels.

At 12:00 UTC (rs10) and 18:00 UTC (rs11) the 27 February, the SBL disappeared to let a well mixed layer from the surface with a residual layer aloft. That appeared accordingly with the wind direction changed and then the advection of air mass from the southwest. As soon as the wind passed from a northerly meridional component to a southerly one, the air temperature decreased (as well as humidity) and the air sea gradient was then inverted after noon, triggered an increase of the THF, thus favoured the turbulent mixing of the lower part of the MABL.

OSD
9, 1387–1436, 2012

Finally, before the synoptic system arrival, one can observe a MABL stabilized by the northwesterly warm and wet air advection. When the synoptic system passed over the ship, the MABL was destabilized by the dynamics and the change in the air advection. The former triggered a dynamic mixing at the MABL top while the latter enhanced the heat release at the base of the MABL inducing a thermal vertical mixing. As a result, a deepening of the mixed layer (up to 900 hPa) was actually observed. Consequently, the sampling of an entire diurnal cycle north of the SAF (rs8 to rs11) does not show evidence of a diurnal cycle effect in the vertical mixing that seems dominated by the synoptic advection variability.

The ship crossed actually the SAF between the 28 (day 59) and 29 (day 60) February. However, the SST time series (Fig. 2a) did not exhibit an abrupt decrease as expected for this usually marked front because of the presence of the two warm oceanic eddies encountered at this location (see Sect. 2 and Arhan et al., 2011). The S eddy (located from 40.6° S to 42.5° S) had a weak surface SST signature except over its southern part where the SST increase of 1 °C between the early 28 February and the mid morning (see Fig. 7c). The SST time series then present a minimum at 10.7 °C and raises up by 3 °C directly afterwards, corresponding of the northern part of the M eddy (located from 42.7° S to 44° S) which had a clear SST surface signature. The SST within the M eddy core reached nearly 14 °C before the abrupt decrease of 4 °C (29 February morning) when the ship sailed out from the eddy. The air temperature started to decrease from the 27 February and then increased the 28 February. The air temperature decreased between the two eddies when the SST decreased accordingly. However, there is an abrupt air temperature decrease while the SST stayed nearly at 14 °C. After noon, the 28 February, the observed wind direction passed from 290° to 250° (Fig. 7a). Consequently, cold air was advected from the southwest explaining the air temperature decrease. Note that this wind direction variation does not appear in the ECMWF ERA reanalysis product (Fig. 8f, g) since the wind direction change occurred between two reanalysis cycles, between 12:00 UTC and 18:00 UTC. It must be also noticed that once this south-westerly wind event was ended, the air temperature re-increased when

OSD
9, 1387–1436, 2012

the ship reached the southern M eddy border and then decreased again as the extreme southern part of the SAF. In the meantime, at the M southern side, the THF decreased accordingly. No synoptic information can explain this wind direction change. O'Neill et al. (2010) suggested that the wind direction is also sensitive to a SST front as well as the wind speed. The size of the M eddy – diameter of 140 km – and its location compared to the SAF (see Arhan et al., 2011) – can let it considered as a part of the SAF front. O'Neill et al. (2010) suggested that the surface winds turn anticyclonically when surface winds flow from cool to warm SST. This anticyclonic wind rotation was actually observed and its maximum was located at the eddy centre. This wind rotation turned back afterwards and decreased southwards until the southern eddy border, to get again the same wind direction observed outside the eddy.

The Fig. 7c also illustrates that the SST anomaly of the two eddies had influence on the turbulent heat fluxes as well as on the net heat fluxes at the ocean surface. For instance, the S eddy exhibited a slight increase of the turbulent heat flux while the M eddy released more than twice the turbulent heat flux released by the S eddy. Moreover, the net heat fluxes released to the atmosphere by the M eddy reached up to 300 $W m^{-2}$.

The air-sea temperature gradient above the M eddy was inverted as compared to outside the eddy, and induces a release of SHF of 15 $W m^{-2}$ on average, reaching up to 23.6 $W m^{-2}$ from the ocean to the atmosphere (not shown). Over the M eddy, the averaged LHF was 180 $W m^{-2}$ (max: 247 $W m^{-2}$), and strongly contrasts with that outside the eddy (not shown).

Since eddies were crossed during nighttimes, the incoming solar radiations were insignificant and the net heat flux at the ocean surface was mainly due to the surface turbulent fluxes of momentum (SHF and LHF). Consequently, over this region, it is evidence that the mesoscale oceanic turbulences (here as a form of eddies) increase significantly the release of heat in the atmosphere mainly via the LHF.

Three atmospheric soundings were performed above the SAF, from 28 to 29 February (rs12, rs13, rs14), and consequently above the M eddy. The first one was released

OSD
9, 1387–1436, 2012

at the northern side of the eddy, the second in the middle of the core while the third one was released beyond the southern side of the eddy (where the SAF was actually overtaken). The rs12 sounding performed the 28 February at 12:00 UTC exhibits a not well mixed but stable layer (Fig. 3). Figure 7c shows that the air temperature was 12.1 °C and SST was 10.7 °C at 12:00 UTC. Such an air-sea temperature gradient tends to cut off the vertical heat flux from ocean to atmosphere (the turbulent heat flux was low: 23.4 W m^{-2}) and to stabilize the low atmosphere.

The rs13 radiosonde was released above the M eddy core at 19:55 UTC, separated of 70 km from rs12. There is evidence of an unstable atmospheric boundary layer (up to 900 hPa) with a cloud layer aloft (where Rh reached 100 %) between 850 hPa and 900 hPa. The observed instability from the surface was associated with the higher SST in the eddy core. Compared to rs12, the air-sea temperature gradient was inverted (air temperature: 12 °C, SST: 13.62 °C – twice as the gradient observed outside the eddy). That induced a peak in the turbulent heat flux (274 W m^{-2}) (Fig. 7c) with a released of an important amount of heat at the base of the atmospheric boundary layer which induced the vertical instability. This process is stopped by an inversion layer where condensation occurred, with the presence of cloud.

The rs14 atmospheric sounding occurred when the ship already crossed the southern side of the M eddy as well as beyond the SAF. The vertical profile (Fig. 3) exhibits a stable boundary layer (as for rs12) from surface to 950 hPa (with a logarithmic vertical wind profile as expected for stable stratification) with a nearly neutral layer aloft up to 900 hPa. From 850 hPa to 900 hPa a residual layer appears. At this time, the wind flow was again from direction higher than 270° thus, warm and moist air arrived over the colder sea surface inducing a stabilization of the lower MABL.

The Fig. 4 also exhibits a weak vertical variability (for wind direction and intensity) for the rs13 sounding compared to rs12 and rs14 soundings. The wind is mainly southwesterly throughout the rs13 MABL while it is mainly northwesterly in the rs12 and rs14 MABL.

OSD
9, 1387–1436, 2012

4.3 The PF

The PF was crossed between the 8 and 9 March (day 68 and 69 respectively). During this period, there was a 3.5 °C decrease of SST and a 5 °C decrease of air temperature accordingly (Fig. 2a). The magnitude of these temperatures collapses was high enough to change the sign of the air-sea temperature gradient and to trigger a heat exchange from the ocean towards the atmosphere at 19:40 UTC (Figs. 2a and 5). At this time, the turbulent heat fluxes grew significantly during all the night between the 8 and 9 March. The joint analysis of the pressure in Fig. 2a and the ECMWF ERA reanalysis (Fig. 9) reveals that the observed abrupt decrease in air temperature and humidity (Fig. 2) is associated with the occurrence of a low pressure system. This latter induced the direction variation of the observed wind from north-westerly to south-westerly and the advection of cold (link to observed air temperature decrease) and dry air. This advection led the change in the air-sea temperature gradient during the mid night. In the meantime, the turbulent heat flux sign was inverted and the net heat flux released towards the atmosphere grew accordingly.

Note that, at the end of the 8 to 9 March night, the ocean mainly lost heat but when the sun rose, the incoming solar radiation counterbalanced the heat loss.

The radiosondes rs21 and rs22 were released at 18:00 UTC the 8 March (day 68) and 12:00 UTC the 9 March (day 69), respectively. The rs21 profile exhibits a profile of a subcloud mixed layer (cloud at 950 hPa) (Fig. 3). This sounding occurred at the sunset (cut off of the incoming solar radiation) while the turbulent heat flux started to significantly increase and when the ocean started to lose heat (net heat flux < 0). This occurs accordingly with the change in wind direction (from 310° to 200°) inducing advection of colder and drier air above the front. This triggered the increase of turbulent heat fluxes and explains the weak instability observed in the low atmosphere (up to 950 hPa) in the rs21 profile.

Even if the rs22 profile was performed at 12:00 UTC when the incoming solar radiation was important, the southwest wind flux persisted (Fig. 9) and the turbulent heat

OSD
9, 1387–1436, 2012

flux released from ocean to atmosphere was significant compared to the region before and after the PF. The lower atmosphere was thus destabilized and actually exhibited an instable surface layer up to 900 hPa on the rs22 profile.

From the 10 March (day 70) at 06:00 UTC to 11 March (day 71) at 06:00 UTC, four radiosondes (from rs23 to rs26 – see Table 2) were released between the PF and the SACCF. Figure 10 illustrates two synoptic low pressure systems located south of the ship with eastwards displacement. Figure 2a also exhibits two pressure minima between the PF and the SACCF corresponding to the two low pressure systems. The south-westerly winds of the first one persisted until 10 March 12:00 UTC (Fig. 10a, b, c). During the late 10 March afternoon, the second low pressure system (centred closer to the ship compared to the first one) produced westerly wind at 18:00 UTC then north-westerly until 11 March 00:00 UTC as well as a wind speed increase (Fig. 10d, e, f).

The situation described by the reanalysis is validated by the wind and barometric in-situ observations (Fig. 11a, b). Unfortunately, the data collection failed from 10 March 23:46 UTC to 11 March 05:47 UTC. The maximum mean wind measured before that failure reached 21 $m\,s^{-1}$ (strong gale) at 22:30 UTC. Nevertheless, the combination of the ERA reanalysis and the observation before and after the data failure (Figs. 10, 11) let reasonably assume that the wind speed (direction) decreased (moved) from roughly 20 $m\,s^{-1}$ to 15 $m\,s^{-1}$ (from north-westerly to south-westerly). In the meantime, the barometric pressure increased while the relative humidity decreased accordingly with the advection of dry and cold air mass from the south.

It is not surprising that the rs23 sounding at 12:00 UTC presents an unstable layer with a well-mixed and deep (up to 825 hPa) mixed layer aloft (Fig. 3). This mixed layer is composed by a subcloud layer and a cloud layer aloft (from 875 hPa). The rs24 (18:00 UTC) presents a similar profile except a decrease of the BL height. The wind measured at the surface by the radiosondes rs24 (18:00 UTC, 10 March) and rs25 (00:00 UTC, 11 March) did not exceed 15 $m\,s^{-1}$ but for rs25, a strong wind is measured in the very low part of the boundary layer (>25 $m\,s^{-1}$) considered as a signature of the

OSD
9, 1387–1436, 2012

northern part of the strong gale passed over the ship before 22:30 UTC (Figs. 4 and 10).

The rs25 profile (00:00 UTC, 11 March) exhibits a very shallow subcloud stable profile (NBL) with a deep cloud layer aloft (illustrated by the humidity saturation up to 650 hPa height). This is the result of the moist and warm north-westerly flux (Figs. 10e, 11a, b).

The rs26 sonde (06:00 UTC, 11 March) was released when the low pressure system was centred to the southeast of the ship (Fig. 10f) with westerly wind. A shallow subcloud stable layer with a well mix cloud layer aloft (shallower than the one observed in the rs25) composed the BL.

4.4 The SACCF

The SACCF was crossed the 12 March (day 72) just before noon and is illustrated by a sharp 1 °C SST gradient along the ship track (Fig. 2a) during which the turbulent heat flux passed from negative ($-7\,W\,m^{-2}$) to positive ($+14\,W\,m^{-2}$) with a progressive decrease of air temperature accordingly (Fig. 5). These two latter changes are associated with a cold front arrived above the ship at 12:00 UTC the 12 March as revealed by the ECMWF ERA reanalysis (not shown) and the relative humidity abrupt decrease (from 90 to 74 % – Fig. 2a). This is the result of the synoptic situation of a deep low pressure system (located exactly south of the ship the 12 March at 00:00 UTC – 969 hPa) and a high pressure system in the North-West. The cold front remained active until the 13 March at 12:00 UTC ($R_h < 75$ % in Fig. 2a).

The radiosondes released during the SACCF crossing exhibited a significant deepening of the MABL. One radiosonde was released before the SACCF (rs27) at noon the 11 March (day 71), and two were released the 12 March (day 72), at noon (rs28) and at 18:00 UTC (rs29). The MABL deepening from 900 hPa (for rs27) to 800 hPa (for rs28) is associated with the displacement of the cold front belonging to the low pressure system evocated. Once the synoptic system passed, the MABL height decreased accordingly, back to 900 hPa (rs31). Consequently, the deep MABL observed was likely related to

OSD
9, 1387–1436, 2012

a cold front passed at this location a couple of hours before (not shown) rather than to a powerful and efficient vertical mixing. The associated south-westerly dense (and cold) air from the southwest forced the warmer air to rise inducing a deepening of the MABL. This phenomenon is relatively classical over the ocean (Dourado et Peireira, 2001). The deepening of the MABL is thus mainly related to a synoptic feature rather than to a regional ocean eddy effect.

5 Discussions

Three interdependent processes influencing the air-sea exchanges have been evocated previously: the surface heat fluxes, the diurnal cycle and the wind regimes.

The Fig. 2 does not exhibit a predominant magnitude of a diurnal cycle in the variability of the main atmospheric variables. However, the Fig. 5 illustrates the diurnal cycle of the net heat flux at the surface itself driven by the diurnal cycle of the solar radiation. The turbulent heat fluxes do not follow this cycle and are more dependant of other factors such the air-sea temperature gradient and the relative humidity. The air-sea temperature gradient depends itself to the ocean dynamics (producing SST anomalies or not) and to the atmospheric synoptic situation which also drives the humidity advection that influence the potential evaporation. The signature of a diurnal cycle within the MABL is thus questionable over the SO region. The importance of the diurnal cycle for the vertical mixing is not well documented, especially when turbulent heat fluxes (influencing the thermal mixing from the base of the MABL) can vary considerably with synoptic wind variability which can itself produces mixing because of the vertical shear. When considering the net heat flux balance (Fig. 5), one can note that the heat lost from ocean to atmosphere occurred mainly during the night (via turbulent processes), while the gain of heat for the ocean occurred during the day when incoming solar radiation are maximal even if the shortwave radiation decreased as the ship moved southwards towards the pole. That suggests diurnal cycle acting within the low MABL and thus a diurnal cycle of the mixing of the low MABL since the turbulent heat fluxes participate to

OSD
9, 1387–1436, 2012

this mixing (see Sect. 4). However, even if this diurnal cycle is suspected in the vertical mixing (for instance the 10 March case, in Sect. 4.3, with a NBL and an unstable BL during afternoon, which is the classical components of a MABL diurnal cycle mixing) the modulation by the synoptic wind does not let a support for a dominant role of this diurnal cycle in the vertical mixing.

Numerous synoptic systems crossed the ship track each time the oceanic fronts were sampled. Consequently, at event or daily scale, it has been difficult to exhibit a direct front effect on the low level wind dynamics as suggested mainly over midlatitudes, subtropical and tropical regions or within the Agulhas current system by Xie et al., 1998; Chelton et al., 2001, 2004, 2010; O'Neill et al., 2003, 2005; Tokinaga et al., 2005; Song et al., 2006. Moreover, in these studies, the timescale considered for the air-sea interaction was mainly longer than a week or more, precisely to remove high frequency variability. The event time scale was thus completely removed. However, the modulation of the turbulent heat fluxes by the synoptic systems has been underlined in Sect. 4 with the in-situ data recorded. The wind direction changes induced changes in the characteristic of the air masses advected in terms of temperature and humidity which directly control the surface heat flux variability that participate to the mixing of the low MABL. The Fig. 2b illustrates that, north of the STF, the mean wind intensity was low (6.3 m s^{-1}) and direction was variable until the 26 February (day 57). From this date and south of the STF until the end of the leg at 57.3° S, the ship sailed in the roaring forties and beyond. The mean wind intensity then became 13.3 m s^{-1} with a mean wind direction of 269.4°. The wind remained mainly westerly with some variation between north-westerly and south-westerly according to the eastwards displacement of the synoptic atmospheric features. The northerly or southerly meridional wind component is the main factor of the wind modulation on the turbulent heat fluxes: the southwards (northwards) wind brought subtropical warm and moist (polar cold and dry) air over colder (warmer) SST which considerably inhibits (enhances) the turbulent heat fluxes magnitude.

OSD
9, 1387–1436, 2012

Moreover, the vertical wind profile (also dependent to the synoptic situation) can also produce its own dynamical vertical mixing and it is interesting to identify the major contributor of the vertical mixing (induced by turbulence) between the wind shear and the thermal flux. The bulk Richardson number (Ri_b) can be useful because it is the ratio of thermal (convective static stability) to mechanical (production/destruction) of turbulent kinetic energy. For instance, the rs1 profile performed during the higher convective activity at 16:21 UTC, above the STF, exhibited an unstable profile with a large negative Ri_b (−6.7), indicating that the flow at the surface was mainly turbulent and unstable due to buoyancy and thermal effect rather than to a shear effect. The turbulent heat flux was enhanced by the south-easterly wind (weak for this region) with dry and cold air. This south-easterly wind thus destabilized the BL by enhanced the ocean to atmosphere flux. This is in accordance with the previous works about a cold and dry air mass destabilizing the BL at the front warm side when the wind flow is nearly perpendicular to the front (e.g. O'Neill et al., 2010). The opposite situation also occurred (rs11) for a neutral case where the boundary layer was well mixed and with a large positive Ri_b (+20), indicating that the turbulent mixing was mainly driven by the wind shear rather than by the buoyancy. That illustrates that, over these regions, the wind can directly inhibits or enhances the vertical mixing by the vertical shear profile.

It is also remarkable to classify the soundings in two categories whatever their geographical locations. The first one contains the soundings for which the SST exceeds the temperature of the air aloft (rs1, rs2, rs3, rs4, rs5, rs13, rs15, rs16, rs22, rs23, rs36) and the soundings for which the air temperature exceeds the SST (rs7, rs8, rs9, rs14, rs17, rs31, rs32) – refer to Fig. 2. It is not surprising that, for the former category, the MABL presents an unstable vertical profile covered by an inversion, mostly around 800 hPa (±50 hPa) (Fig. 3) and, for the latter category the MABL presents a near stable profile which indicates that the vertical mixing is inhibited or completed with a significant vertical extend. But as evocated before, the air-sea temperature gradient is mainly controlled by the wind direction associated with the synoptic system displacements.

OSD
9, 1387–1436, 2012

The particular case of the M eddy has been sampled during this cruise and a similar Agulhas eddy (centred at ~42° S–20° E) has been sampled in June–July 1993 (Rouault and Lutjeharms, 2000). This latter released 500 W m^{-2} as latent heat fluxes and 350 W m^{-2} as sensible heat flux compared to the 250 W m^{-2} of the M eddy turbulent heat fluxes. The 1993 eddy had somewhat the same origins as eddy M, but was likely younger, which explains the huge difference in term of heat flux measured for these two eddies. It had a surface temperature up to ~17 °C and a 250 m-thick mixed layer, whereas eddy M has surface temperatures slightly below 14 °C, and a ~50 m summer mixed layer. The direct and derived atmospheric measurements above the M eddy presented in this paper permitted to describe some thermodynamic effects of the M eddy on the vertical atmosphere aloft. The warm SST anomaly of the eddy core induced a vertical destabilization of the atmosphere by increasing the vertical turbulent heat transfer from the ocean to the atmosphere (when the air temperature is lower than the SST). This transfer is mainly driven by the latent heat flux rather than the sensible heat flux. This latter is roughly five times less efficient than the former (see Fig. 16 in Arhan et al., 2011) because of the lower relative humidity above the eddy centre (Fig. 7b) due mainly to the south-westerly wind rotation during the measurement.

6 Conclusions

The Southern Hemisphere south of south Africa has received little attention as regard air-sea interaction, most likely due to paucity of measurements associated with harsh weather conditions. The measurements performed during the BONUS-GOODHOPE 2008 cruise provided a continuous sampling of the atmospheric state close to the ocean surface (from 34.4° S/15.9° E to 57.55° S/00° E) as well as vertical samplings of the atmosphere where the radiosondes were released regularly and/or over remarkable oceanic features (fronts, eddies). Additionally, the in-situ atmospheric data permitted to derive the turbulent heat flux and finally the heat balance at the surface by also considering the measured radiation terms. To the author knowledge, it is the first time that

OSD
9, 1387–1436, 2012

such atmospheric measurements have been conducted along this north-south track that crossed major oceanic fronts from South Africa to 57° S.

The joint analysis of this in-situ dataset and the ECMWF reanalysis for the determination of the synoptic conditions leads to the following conclusions:

- The STF, SAF and PF fronts encountered during the cruise exhibited some sharp SST gradients and it has been shown that the MABL vertical structure is subject to significant variability, especially over the warm side of the SST fronts with stabilization or destabilization associated with the synoptic systems passed over.

- The stability of the MABL is the result of the combined thermal and mechanical processes that can mix or not the MABL. The thermal processes occurred mainly from the surface by the turbulent heat fluxes transfers while the mechanical processes due the wind shear were able to mix within the entire BL. However, the former is also partly controlled by the dynamics. Consequently, it has been shown that, south of the STF, the meridional component of the wind drives the stability variability of the MABL by an enhancement or an inhibition of the surface thermal processes and the wind shear. Since the SST gradient and the sharp SST front are North-South organized, and since the zonal wind is mainly westerly: (i) a northerly meridional wind induces a stabilization of the MABL over the warm side of the front and, (ii) a southerly meridional wind induces a destabilization of the MABL over the warm side of the front.

- The synoptic systems, by their wind rotation associated to the Coriolis effect, control the meridional wind variability because such systems continuously turn around the Antarctic continent.

- The direct impact of the warm eddy on the MABL has been shown in terms of thermodynamics effect mainly through the turbulent heat fluxes. Some dynamics effects were suspected (anticyclonic wind rotation above the warmer SST – eddy centre) but a higher spatial resolution sampling was required to demonstrate this

OSD
9, 1387–1436, 2012

actual effect of the eddy. The lack of information about the synoptic situation at the exact time of measurements complicates the analysis and does not permit to discriminate whether or not the eddy impacts mainly the atmospheric surface dynamics.

Finally, the wind changes, associated with the eastwards displacement of synoptic features, induced northerly (southerly) advection of warm (cold) and moist (dry) air above colder (warmer) water presenting a high SST gradient. The result was a decrease (increase) of the turbulent heat flux above these SST discontinuities, stabilizing (destabilizing) the MABL just above (see Fig. 12). Additionally, according to the vertical wind shear profile and the wind intensity, these processes can be enhanced or inhibited.

These conclusions based on observation strengthen and supplement remarks and nuances found in the Small et al. (2008) review about the effects of synoptic system on the MABL stratification.

Additionally, the simple consideration of the mean in situ Bowen ratio (between sensible and latent heat fluxes) along the summertime BGH cruise (0.041) indicates that a major part of the available energy at the ocean surface is passed to the atmosphere through evaporative processes. The evaporative fraction (0.96 over the whole cruise) is then appropriate for representing the relative contributions of the turbulent heat fluxes to the heat budget. During that summer, the latent heat flux was mainly released from ocean to atmosphere. Consequently, the ocean mainly lost heat through evaporative turbulent processes, which are highly dependent on wind velocity. However, it cannot be concluded that the phenomena is amplified during the winter season. Walker and Mey (1988) indeed showed that turbulent heat flux display little seasonality over the Agulhas retroflexion region. The main reason is persistent westerly and south-westerly wind flow throughout the year which ensures that cold/dry air repeatedly forces loss of ocean heat. As a consequence, once a SST anomaly is identified and persistent, investigate the frequencies, the intensities and especially the meridional wind component occurrences can bring relevant information for quantifying the loss of ocean heat from South African continent to the ACC.

OSD
9, 1387–1436, 2012

Finally, the dataset recorded during the BGH cruise also presents interest for other studies (atmospheric reanalysis assessment, air-sea processes over southern ocean, etc.) and were already used to validate two satellite data sets: the twice daily QuikSCAT winds and the daily OAflux data set of latent and sensible heat fluxes as well as numerical weather forecasts performed during the cruise with the WRF model over the Southern Ocean (Messager et Faure, 2012).

Acknowledgements. Authors are thankful to the officers and crew of the R/V *Marion Dufresne*, for their precious help and cooperation, and to all other contributors to the numerous measurements used in the article. The IPY/BONUS-GoodHope and CLIVAR/GoodHope projects received support from the Institut National des Sciences de l'Univers (INSU), the CNRS, the IFREMER program "*Circulation Océanique*", the French Polar Institute Paul Emile Victor (IPEV), the University of Brest (UBO-IUEM), and the and the *Agence Nationale de la Recherche* (ANR) (ANR-07-BLAN-0146-01). The LOS-IFREMER is also thanks because of the funds provided for the radiosoundings.

The publication of this article is financed by CNRS-INSU.

References

Ansorge, I., Speich, S., Lutjeharms, J., Goni, G., Rautenbach, H., Froneman, W., Garzoli, S., and Arhan, M.: Monitoring the oceanic flow between Africa and Antarctica: Report of the first GoodHope cruise, J. of African Science, 100, 319–323, 2004.

OSD
9, 1387–1436, 2012

Arhan, M., Speich, S., Messager, C., Dencausse, G., Fine, R., and Boye, M.: Anticyclonic and cyclonic eddies of subtropical origin in the subantarctic zone south of Africa, J. Geophys. Res., 116, C11004, doi:10.1029/2011JC007140, 2011.
Belkin, I. M. and Gordon, A. L.: Southern Ocean fronts from the Greenwich meridian to Tasmania, J. Geophys. Res., 101, 3675–3696, 1996.
Boebel, O., Lutjeharms, J., Schmid, C., Zenke, W., Rossby, T., and Barron, C.: The Cape Cauldron: a regime of turbulent inter-ocean exchange, Deep-Sea Res. II, 50, 57–86, 2003.
Bourras, D., Reverdin, G., Giordani, H., and Caniaux, G.: Response of the atmospheric boundary layer to a mesoscale oceanic eddy in the northeast Atlantic, J. Geophys. Res., 109, D18114, doi:10.1029/2004JD004799, 2004.
Businger, J. A. and Shaw, W. J.: The response of the marine boundary layer to mesoscale variations in sea-surface temperature, Dyn. Atmos. Oceans, 8, 267–281, 1984.
Chelton, D. B. and Xie, S.-P.: Coupled ocean-atmosphere interaction at oceanic mesoscales, Oceangr. Mag., 4, 52–69, 2010.
Chelton, D. B., Esbensen, S. K., Schlax, M. G., Thum, N., and Freilich, M. H.: Observations of coupling between surface wind stress and sea surface temperature in the eastern tropical Pacific, J. Climate, 14, 1479–1498, 2001.
Chelton, D. B., Schlax, M. G., Freilich, M. H., and Milliff, R. F.: Satellite measurements reveal persistent small-scale features in ocean winds, Science, 303, 978–983, 2004.
De Mey, R., Walker, N., and Jury, M.: Surface Heat Fluxes and Marine Boundary Layer Modification in the Agulhas Retroflection Region, J. Geophys. Res., 95, 15997–16015, 1990.
Dencausse, G., Arhan, M., and Speich, S.: Spatio-temporal characteristics of the Agulhas Current Retroflection, Deep Sea Res. I, 57, 1392–1405, 2010.
De Ruijter, W. P. M., Biastoch, A., Drijfhout, S. S., Lutjeharms, J. R. E., Matano, R. P., Pichevin, T., Van Leeuwen, P. J., and Weijer, W.: Indian-Atlantic interocean exchange: Dynamics, estimation and impact, J. Geophys. Res., 104, 20885–20910, 1999.
Dourado, M. and Peireira de Oliveira, A.: Observational description of the atmospheric and oceanic boundary layers over the Atlantic ocean, Re. Bras. Oceanogr., 49, 49–59, 2001.
Duncombe Rae, C. M.: Agulhas Retroflection Rings In the South Atlantic Ocean: An Overview, S. Afr. J. Mar. Sci., 11, 327–344, 1991.
Fairall, C. W., Bradley, E. F., Hare, J. E., Grachev, A. A., and Edson, J. B.: Bulk parameterization on air–sea fluxes: Updates and verification for the COARE algorithm, J. Climate, 16, 571–591, 2003.

OSD
9, 1387–1436, 2012

Faure, V., Arhan, M., Speich, S., and Gladyshev, S.: Heat budget of the surface mixed layer south of Africa, Ocean Dynam., 61, 1441–1458, 2011

Friehe C. A., Shaw, W. J., Rogers, D. P., Davidson, K. L., Large, W. G., Stage, S. A., Crescenti, G. H., Khalsa, S. J. S., Greenhut, G. K., and Li, F.: Air–sea fluxes and surface layer turbulence around a sea-surface temperature front, J. Geophys. Res., 96, 8593–8609, 1991.

Giordani, H., Planton, S., Benech, B., and Kwon, B.-H.: Atmospheric boundary layer response to sea surface temperatures during the SEMAPHORE experiment, J. Geophys. Res., 103, 25047–25060, 1998.

Gladyshev, S., Arhan, M., Sokov, A., and Speich, S.: A hydrographic section from South Africa to the southern limit of the Antarctic Circumpolar Current at the Greenwich meridian, Deep Sea Res., 55, 1284–1303, 2008.

Gordon, A. L.: Indian-Atlantic transfer of thermocline water at the Agulhas retroflection, Science, 227, 1030–1033, 1985.

Jury, M. R. and Walker, N.: Marine boundary layer modification across the edge of the Agulhas Current, J. Geophys. Res., 93, 647–654, 1988.

Kelly, K. A., Small, R. J., Samelson, R. M., Qiu, B., Joyce, T. M., Kwon, Y. O., and Cronin, M. F.: Western boundary currents and frontal air-sea interaction: Gulf Stream and Kuroshio extension, J. Climate, 23, 5644–5667, 2010.

Kwon, B.-H., Bénech, B., Lambert, D., Durand, P., Druilhet, A., Giordani, H., and Planton, S.: Structure of the marine atmospheric boundary layer over an oceanic thermal front: SEMAPHORE experiment, J. Geophys. Res., 103, 25159–25180, 1998.

Kwon, Y. O., Alexander, M. A., Bond, N. A., Frankignoul, C., Nakamura, H., Qiu, B., and Thompson, L. A.: Role of Gulf Stream and Kuroshio-Oyashio systems in large-scale atmosphere-ocean interaction: A review, J. Climate, 23, 3249–3281, 2010.

Lee-Thorp, A. M., Rouault, M., and Lutjeharms, J. R. E.: Moisture uptake in the boundary layer above the Agulhas Current: A case study, J. Geophys. Res., 104, 1423–1430, 1999.

Lutjeharms, J. R. E.: The Agulhas Current, Springer, 2006.

Lutjeharms, J. R. E.: The exchange of water between the South Indian and South Atlantic Ocean, in: The South Atlantic: Present and Past Circulation, edited by: Wefer, G., Berger, W. H., Siedler, G., and Webb, D. J., Berlin (Springer-Verlag), 125–162, 1996.

Lutjeharms, J. R. E. and Gordon, A. L.: Shedding of an Agulhas ring observed at sea, Nature, 325, 138–140, 1987.

OSD

9, 1387–1436, 2012

Lutjeharms, J. R. E. and Valentine, H. R.: Eddies at the Subtropical Convergence South of Africa, J. Phys. Ocean., 18, 761–774, doi:10.1175/1520-0485(1988)018<0761:EATSCS>2.0.CO;2, 1988.
Lutjeharms, J. R. E. and Van Ballegooyen, R. C.: The retroflexion of the Agulhas Current, J. Phys. Ocean., 18, 1570–1583, 1988.
Messager, C. and Faure, V.: Validation of remote sensing and weather model forecasts in the Agulhas ocean area to 57° S by ship observations, S. Afr. J. Sci., 108, 1–10, doi:10.4102/sajs.v108i3/4.735, 2012.
Minnett, P. J., Knuteson, R. O., Best, F. A., Osborne, B. J., Hanafin, J. A., and Brown, O. B.: The Marine-Atmosphere Emitted Radiance Interferometer (M-AERI), a high-accuracy, sea-going infrared spectroradiometer, J. Atmos. Ocean. Tech., 18, 994–1013, 2001.
Morrow, R., Birol, F., Griffin, D., and Sudre, J.: Divergent pathways of cyclonic and anti-cyclonic ocean eddies, Geophys. Res. Lett., 31, L24311, doi:10.1029/2004GL020974, 2004.
O'Neill, L. W., Chelton, D. B., and Esbensen, S. K.: High-Resolution Satellite Measurements of the Atmospheric Boundary Layer Response to SST Variations along the Agulhas Return Current, J. Climate, 18, 2706–2723, 2005.
O'Neill, L. W., Chelton, D. B., and Esbensen, S. K.: The Effects of SST-Induced Surface Wind Speed and Direction Gradients on Midlatitude Surface Vorticity and Divergence, J. Climate, 23, 255–281, 2010.
Orsi, A. H., Whitworth III, T., and Nowlin, W. D.: On the meridional extent and fronts of the Antarctic Circumpolar Current, Deep-Sea Res. I, 42, 641–673, 1995.
Orsi, A. H., Nowlin Jr., W. D., and Whitworth III, T.: On the circulation and stratification of the Weddell Gyre, Deep-Sea Res. I, 40, 169–203, 1993.
Phillips, H. E. and Rintoul S. R.: Eddy Variability and Energetics from Direct Current Measurements in the Antarctic Circumpolar Current South of Australia, J. Phys. Ocean., 30, 3050–3076, doi:10.1175/1520-0485(2000)030<3050:EVAEFD>2.0.CO;2, 2000.
Reason, C. J. C.: Evidence for the influence of the Agulhas Current on regional atmospheric circulation patterns, J. Climate, 14, 2769–2778, 2001.
Rouault, M. and Lee-Thorp, A. M.: Fine-time resolution measurements of atmospheric boundary layer properties between Cape Town & Marion Island, S. Afr. Mar. Sci., 17, 281–296, 1996.
Rouault, M. and Lutjeharms, J. R. E.: Air-sea exchanges over an Agulhas eddy at the subtropical convergence, Global Atmos.-Ocean Syst., 7, 125–150, 2000.

OSD
9, 1387–1436, 2012

Rouault, M., Lee-Thorp, A. M., Ansorge, I., and Lutjeharms, J. R. E.: Agulhas Current Air-Sea Exchange Experiment, S. Afr. J. Sci., 91, 493–496, 1995.
Rouault, M., Lee-Thorp, A. M., and Lutjeharms, J. R. E.: The atmospheric Boundary Layer above the Agulhas Current during Alongcurrent Winds, J. Phys. Oceanogr., 30, 40–50, 2000.
Schouten, M. W., de Ruijter, W. P. M., van Leeuwen, P. J., and Lutjeharms, J. R. E.: Translation, decay and splitting of Agulhas rings in the south-eastern Atlantic Ocean, J. Geophys. Res., 105, 21913–21925, 2000.
Small, R. J., DeSzoeke, S. P., Xie, S. P., O'Neill, L., Seo, H., Song, Q., Cornillon, P., Spall, M., and Minobe, S.: Air-sea interaction over ocean fronts and eddies, Dynam. Atmos. Oceans, 45, 274–319, 2008.
Stammer, D.: On Eddy Characteristics, Eddy Transports, and Mean Flow Properties, J. Phys. Ocean., 28, 727–739. doi:10.1175/1520-0485(1998)028<0727:OECETA>2.0.CO;2, 1998.
Sokolov, S. and Rintoul, S. R.: Circumpolar structure and distribution of the Antarctic Circumpolar Current fronts: 1. Mean circumpolar paths, J. Geophys. Res., 114, C11018, doi:10.1029/2008JC005108, 2009a.
Sokolov, S. and Rintoul, S. R.: Circumpolar structure and distribution of the Antarctic Circumpolar Current fronts: 2. Variability and relationship to sea surface height, J. Geophys. Res., 114, C11019, doi:10.1029/2008JC005248, 2009b.
Song, Q., Cornillon, P., and Friehe, C. A.: Surface wind response to oceanic fronts, J. Geophys. Res., 111, C12006, doi:10.1029/2006JC003680, 2006.
Spall, M. A.: Midlatitude wind stress-sea surface temperature coupling in the vicinity of ocean fronts, J. Climate, 20, 3785–3801, 2007.
Speich, S. and Dehairs, F.: Cruise Report, MD 166 BONUS-GOODHOPE, *Internal Report*, 246 pp., 2008.
Swart, S. and Speich, S.: An altimetry-based gravest empirical mode south of Africa: 2. Dynamic nature of the ACC fronts, J. Geophys. Res., 115, C03003, doi:10.1029/2009JC005300, 2010.
Swart, S., Speich, S., Ansorge, I., Goni, G., Gladyshev, S., and Lutjeharms, J.: Transport and variability of the antarctic circumpolar current South of Africa, J. Geophys. Res., 113, C09014, doi:10.1029/2007JC004223, 2008.
Tokinaga, H., Tanimoto, Y., and Xie, S.-P.: SST–induced surface wind variations over the Brazil–Malvinas Confluence: Satellite and in situ observations, J. Climate, 18, 3470–3482, 2005.

OSD
9, 1387–1436, 2012

Tokinaga, H., Tanimoto, Y., Nonaka, M., Taguchi, B., Fukamachi, T., Xie, S.-P., Nakamura, H., Watanabe, T., and Yasuda, I.: Atmospheric sounding over the winter Kuroshio Extension: Effect of surface stability on atmospheric boundary layer structure, Geophys. Res. Lett., 33, L04703, doi:10.1029/2005GL025102, 2006.

Walker, M. and De Mey, R.: Ocean/atmosphere heat fluxes within the agulhas retroflection region, J. Geophys. Res., 93, 15473–15483, 1988.

White, W. B. and Annis, J. L.: Coupling of extratropical mesoscale eddies in the ocean to westerly winds in the atmospheric boundary layer, J. Climate, 33, 1095–1107, 2003.

Xie, S.-P., Ishiwatari, M., Hashizume, H., and Takeuchi, K.: Coupled ocean–atmosphere waves on the equatorial front, Geophys. Res. Lett., 25, 3863–3866, 1998.

OSD

9, 1387–1436, 2012

Table 1. Instrument Characteristics.

Manufacturer	Instrument	Height	Parameters	Units	Uncertainty	Sampling Rate
Space Science and Engineering	M-AERI	20 m	Skin-Temperature	°C	< 0.1[1]	10 min
Center, University of Wisconsin-Madison			Air Temperature	°C	<0.1[1]	10 min
Coastal Environmental Systems. Inc.	Wind vane 5103	20 m	Wind speed and direction	$m\,s^{-1}$ °	±0.3[2] ±3[2]	1 min
	Relative Humidity S1057W	20 m	Relative humidity	%	±2[3]	1 min
	Barometer 6400	20 m	Barometric pressure	hPa	±0.5[4]	1 min
	Temperature S1074		Air Temperature	°C	±0.1	1 min
Eppley Laboratory	Precision Infrared radiometer	20 m	Longwave radiation	$W\,m^{-2}$	<5 %	1 min
	Prescision Spectral Pyranometer	20 m	Shortwave radiation	$W\,m^{-2}$	±1 %	1 min
SeaBird	Thermo-salinograph	−6 m	Sea Bulk temperature	°C	±0.01	1 min
Vaisala	Radiosondes RS92-SGP	From 14 m to 29 000 m	Vertical profile of air temperature	°C	±0.15[6]	1 min to 10 min[7]
		From 14 m to 29 000 m	Vertical profile of air humidity	%	±2 %[6]	1 min to 10 min[7]
		From 14 m to 29 000 m	Vertical profile of wind direction	°	±2[6]	1 min to 10 min[7]
		From 14 m to 29 000 m	Vertical profile of wind speed	$m\,s^{-1}$	±0.15[6]	1 min to 10 min[7]
		From 14 m to 29 000 m	Vertical profile of barometric pressure	hPa	±0.4 hPa	1 min to 10 min[7]

[1] Minnett et al. (2001). [2] Coastal Environmental Systems, Inc., Wind Monitor 5103 brochure. [3] Coastal Environmental Systems, Inc., Relative Humidity Sensor S1057 brochure. [4] Coastal Environmental Systems, Inc., Barometer 6400 brochure. [5] ARM MWR manual for December conditions at the SGP site. [6] All radiosonde uncertainties are based on repeatability in calibration from Vaisälä. [7] For radiosonde data collected before 4 March 2008, the sampling interval for all radiosonde variables was 10 s.

OSD
9, 1387–1436, 2012

Table 2. Times and locations of the 38 radiosondes released. The information column indicates locations of fronts and measurement of diurnal cycles.

Sondes	Date	Day/1Jan	Time	Latitude	Longitude	Information
RS1	2008.02.23	54	16:21	38.09° S	12.09° E	STF
RS2	2008.02.24	55	11:45	39.19° S	11.32° E	
RS3	2008.02.24	55	18:02	39.56° S	11.06° E	
RS4	2008.02.25	56	11:50	40.72° S	10.21° E	
RS5	2008.02.25	56	17:59	41.18° S	9.92° E	
RS6	2008.02.26	57	11:55	42.04° S	9.27° E	
RS7	2008.02.26	57	17:57	42.25° S	9.10° E	
RS8	2008.02.26	57	23:55	42.47° S	8.93° E	Diurnal Cycle at a stopped station
RS9	2008.02.27	58	06:12	42.47° S	8.93° E	
RS10	2008.02.27	58	11:55	42.47° S	8.93° E	
RS11	2008.02.27	58	17:56	42.47° S	8.93° E	
RS12	2008.02.28	59	11:55	42.78° S	8.67° E	SAF
RS13	2008.02.28	59	19:55	43.32° S	8.24° E	
RS14	2008.02.29	60	08:01	44.04° S	7.63° E	
RS15	2008.03.01	61	16:04	44.90° S	6.89° E	
RS16	2008.03.03	63	11:55	46.36° S	5.54° E	
RS17	2008.03.04	64	12:05	47.51° S	4.41° E	
RS18	2008.03.05	65	17:58	47.55° S	4.38° E	
RS19	2008.03.06	66	11:59	47.97° S	3.96° E	
RS20	2008.03.07	67	11:53	49.03° S	2.83° E	
RS21	2008.03.08	68	18:13	50.11° S	1.61° E	PF
RS22	2008.03.09	69	12:14	50.64° S	0.86° E	
RS23	2008.03.10	70	11:56	51.85° S	0.00° E	Diurnal Cycle at a stopped station
RS24	2008.03.10	70	17:54	51.86° S	0.00° E	
RS25	2008.03.10	70	23:55	51.86° S	0.00° E	
RS26	2008.03.11	71	06:07	51.88° S	0.01° E	
RS27	2008.03.11	71	11:55	51.89° S	0.00° E	SACCF
RS28	2008.03.12	72	11:55	52.98° S	0.00° E	
RS29	2008.03.12	72	17:57	53.26° S	0.00° E	
RS30	2008.03.13	73	11:55	54.71° S	0.07° W	
RS31	2008.03.14	74	12:04	55.67° S	0.03° E	
RS32	2008.03.15	75	05:58	56.74° S	0.00° E	
RS33	2008.03.15	75	17:51	57.55° S	0.04° W	
RS34	2008.03.15	75	23:54	57.55° S	0.04° W	
RS35	2008.03.16	76	05:53	57.55° S	0.04° W	
RS36	2008.03.16	76	11:55	57.55° S	0.04° W	
RS37	2008.03.16	76	17:53	57.55° S	0.04° W	
RS38	2008.03.17	77	11:56	57.55° S	0.04° W	

OSD
9, 1387–1436, 2012

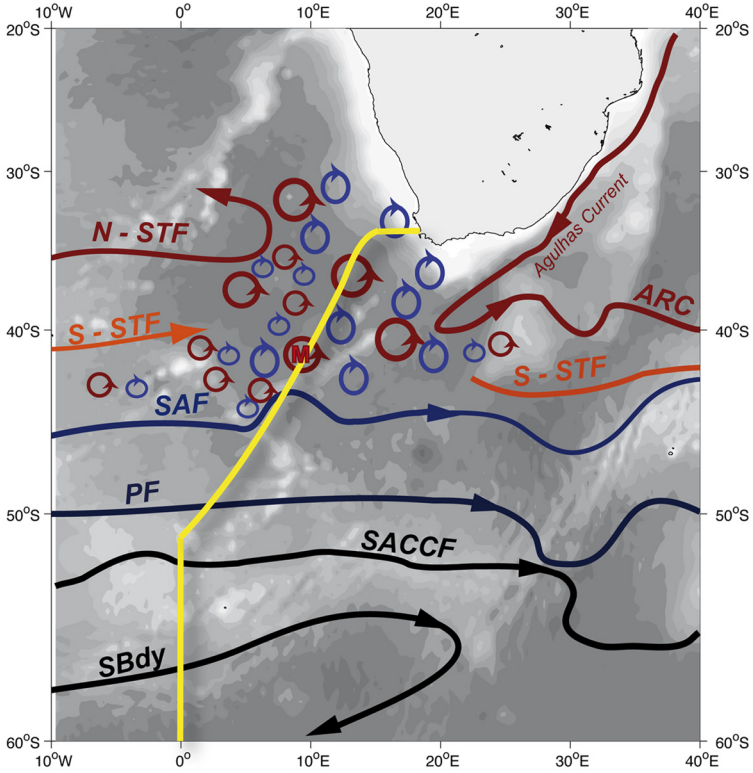

Fig. 1. Fronts location (for the period 15 February–20 March 2008) based on satellite altimetry. ARC is the Agulhas Return Current; N-STF and S-STF are the Northern and the Southern Subtropical Front (STF) respectively; SAF is the Subantarctic Front, PF is the Polar Front, SACCF is the Southern ACC front and SBy is the Southern Boundary. Also shown are the ship track (yellow line) and the location of the "M" eddy (see text).

OSD
9, 1387–1436, 2012

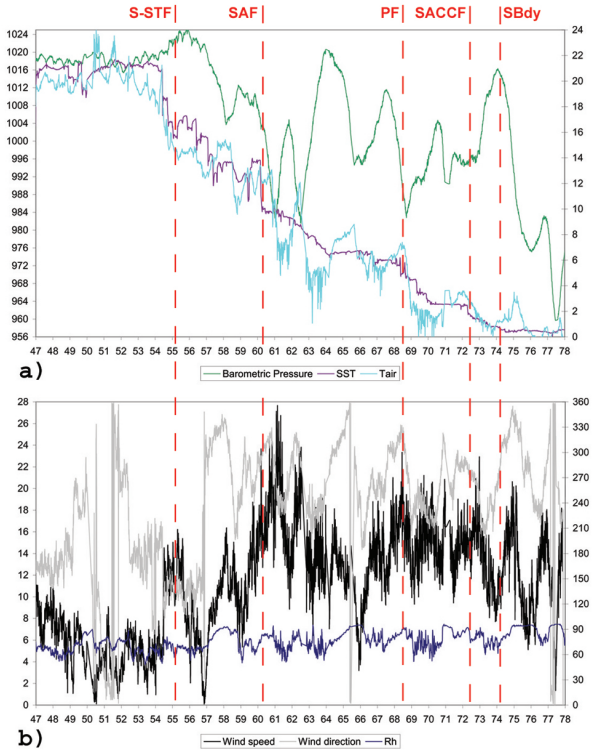

Fig. 2. Time series of **(a)** the barometric pressure in hPa (green line), the SST and Air temperature at ten meters height in ˚C (purple and blue lines respectively) and; **(b)** wind speed in m s^{-1} and wind direction (black and grey lines respectively) as well as relative humidity (dark blue line) in %. For **(a)**, left vertical scale is pressure in hPa and right vertical scale is temperature in ˚C. For **(b)** left vertical scale is wind speed in m s^{-1} and right vertical scale is direction in degree as well as relative humidity in %. The vertical dashed red lines are the location of the oceanic fronts.

OSD
9, 1387–1436, 2012

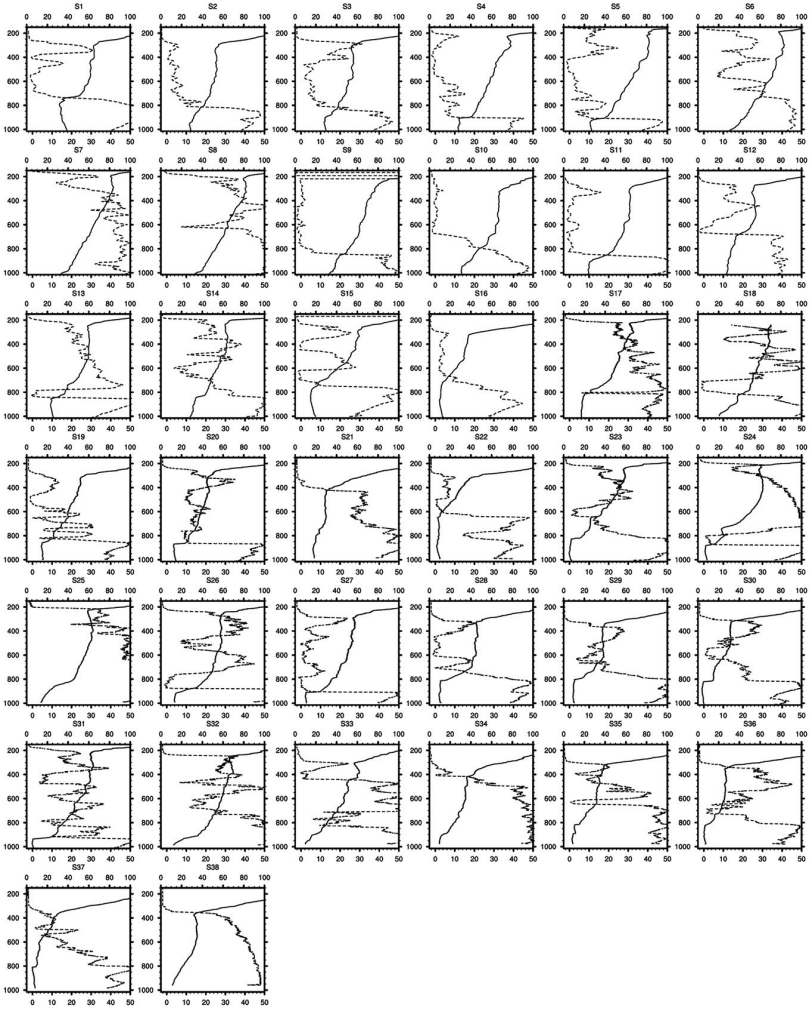

Fig. 3. Caption on next page.

OSD
9, 1387–1436, 2012

Fig. 3. Vertical profile of potential temperature – ˚C – (bold line) and relative humidity – % – (dashed line) for the 38 radiosondes. For locations, dates and times see Table 2.

OSD
9, 1387–1436, 2012

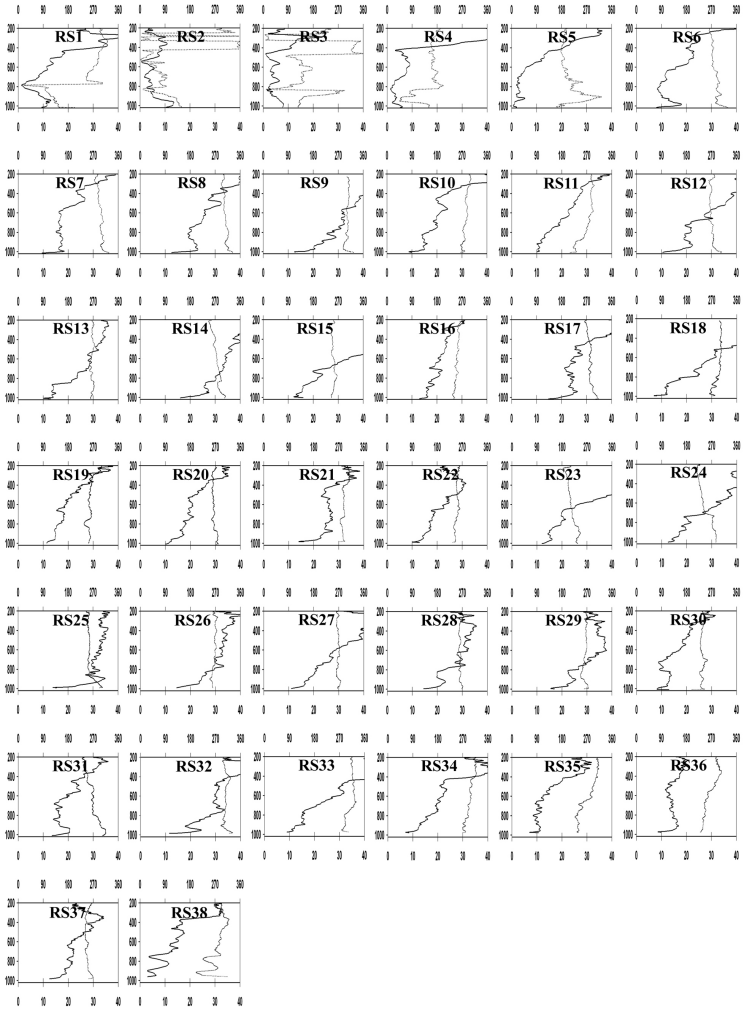

Fig. 4. Caption on next page.

OSD
9, 1387–1436, 2012

Fig. 4. Vertical profile of wind speed – $m\,s^{-1}$ – (bold line) and wind direction – deg – (dashed line) for the 38 radiosondes. For locations, dates and times see Table 2.

OSD
9, 1387–1436, 2012

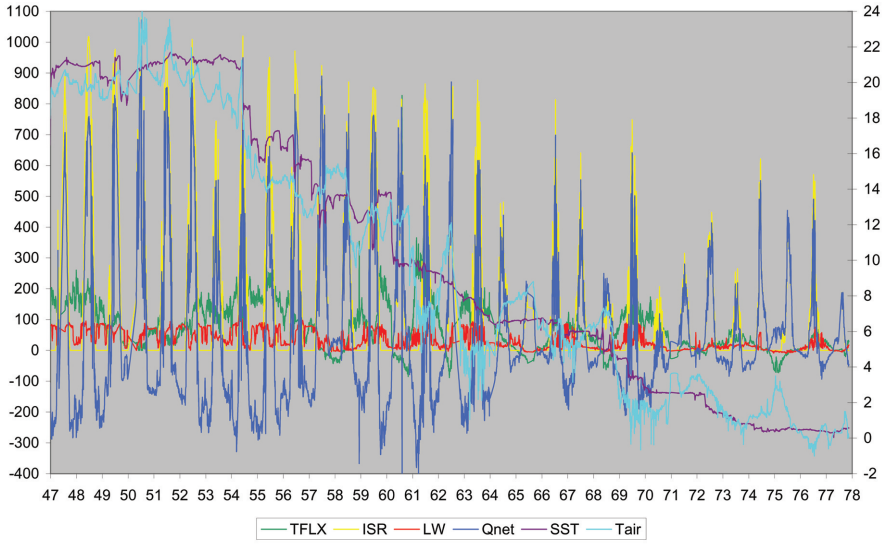

Fig. 5. Time series for turbulent heat fluxes (green curve) – positive upward, incoming solar radiation (yellow curve) – positive downward, longwave radiation (red curve) – positive upward, net heat flux (dark blue curve) – negative upward, SST (purple curve) and air temperature (light blue curve). Left vertical axe is heat flux in W m^{-2} and right vertical axe is temperature in °C.

OSD
9, 1387–1436, 2012

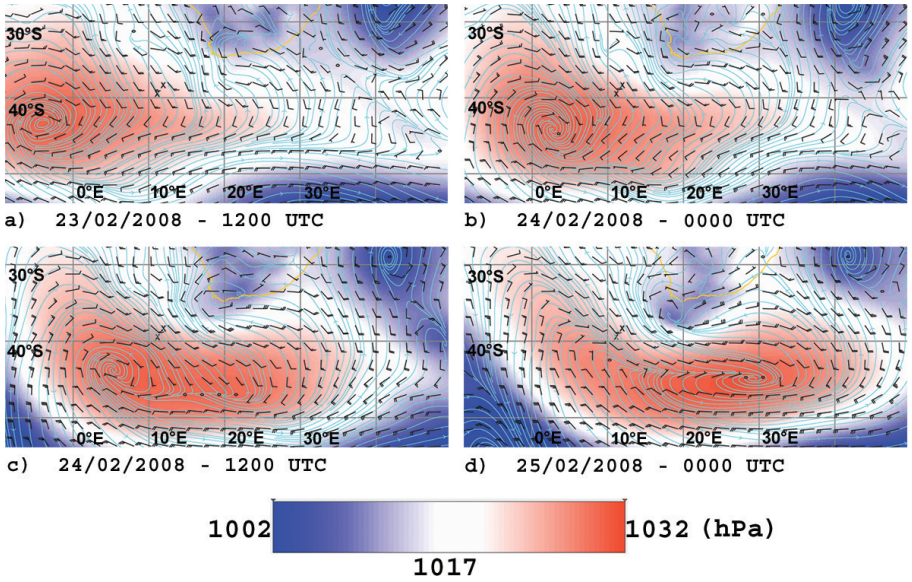

Fig. 6. Synoptic situation when the ship crossed the STF (from ECMWF ERA interim reanalysis). Colored background is the medium sea level pressure, light blue isolines are streamlines at 10 m height. Wind barbs (in knots) are overlaid. Black crosses indicate the rs1 and rs2 release locations. Brown line is the South African coastline.

OSD
9, 1387–1436, 2012

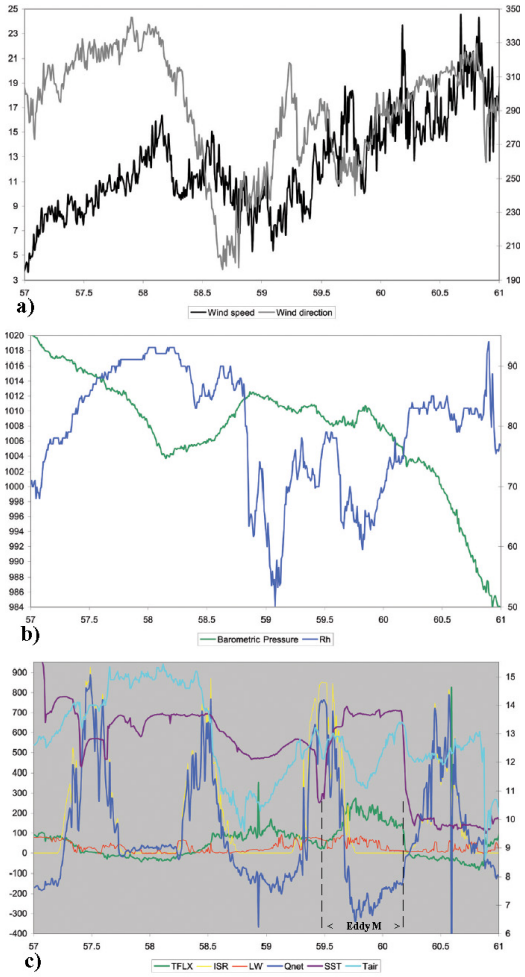

Fig. 7. Caption on next page.

OSD
9, 1387–1436, 2012

Fig. 7. Time series of **(a)** wind speed and wind direction (black and grey lines respectively) in $m\,s^{-1}$ and ° and; **(b)** relative humidity (blue line) in % and barometric pressure (red line) in hPa and; **(c)** turbulent heat fluxes (green curve), incoming solar radiation (yellow curve), longwave radiation (red curve), net heat flux (dark blue curve), SST (purple curve) and air temperature (light blue curve). For **(a)**, left vertical scale is wind speed in $m\,s^{-1}$ and right vertical scale is direction in °. For **(b)**, left vertical axe is pressure in hPa and right vertical axe is relative humidity in %. For **(c)**, left vertical axe is heat flux in $W\,m^{-2}$ and right vertical axe is temperature in °C.

OSD
9, 1387–1436, 2012

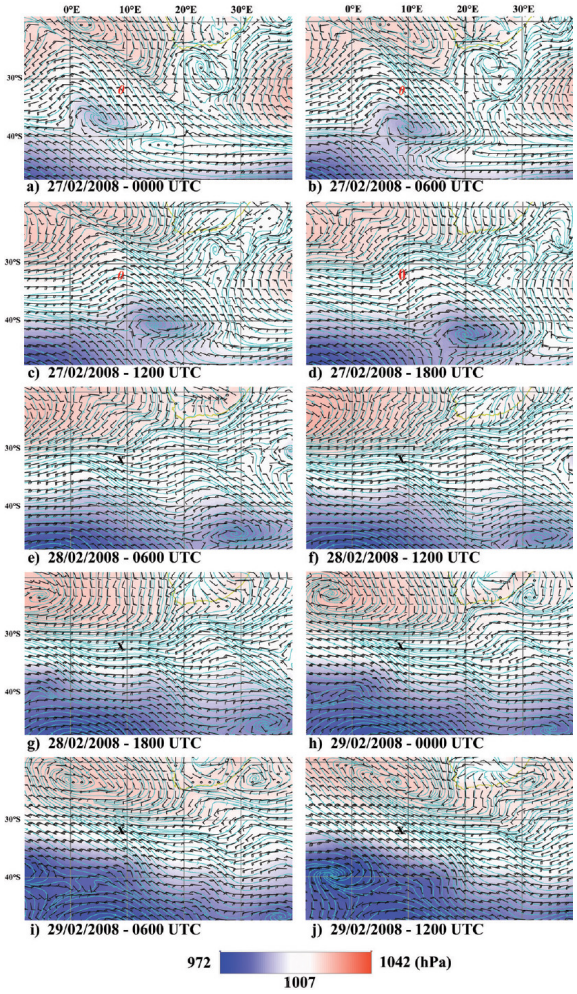

Fig. 8. Caption on next page.

OSD
9, 1387–1436, 2012

Fig. 8. Synoptic situation from the 27 February to the 29 February 2008, before, when and after the ship crossed the SAF (from ECMWF ERA interim reanalysis). Colored background is the medium sea level pressure, light blue isolines are streamlines at 10 m height. Wind barbs (in knots) are overlaid. Red "0" indicates the the ship location (42.47° S/8.93° E) where rs8 to rs11 were released. Black cross indicates the rs12, rs13 and rs14 release locations. Brown line is the South African coastline.

OSD
9, 1387–1436, 2012

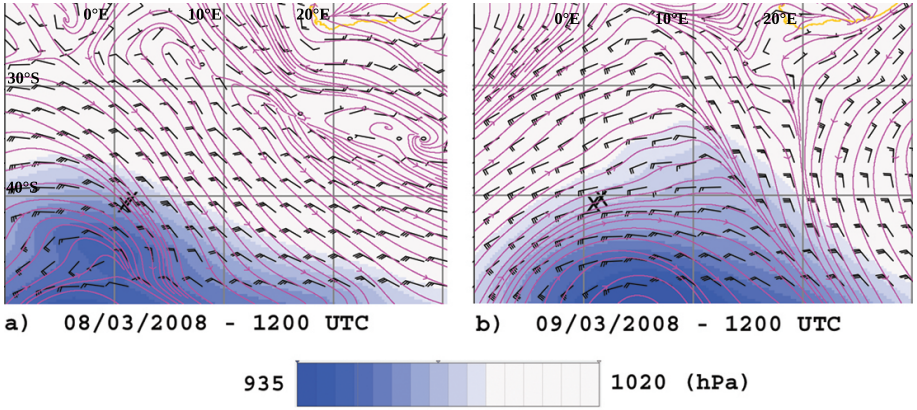

Fig. 9. Synoptic situation when the ship crossed the PF (from ECMWF ERA interim reanalysis). Colored background is the medium sea level pressure, purple isolines are streamlines at 10 m height. Wind barbs (in knots) are overlaid. Black crosses indicate the rs21 and rs22 release locations. Brown line is the South African coastline.

OSD
9, 1387–1436, 2012

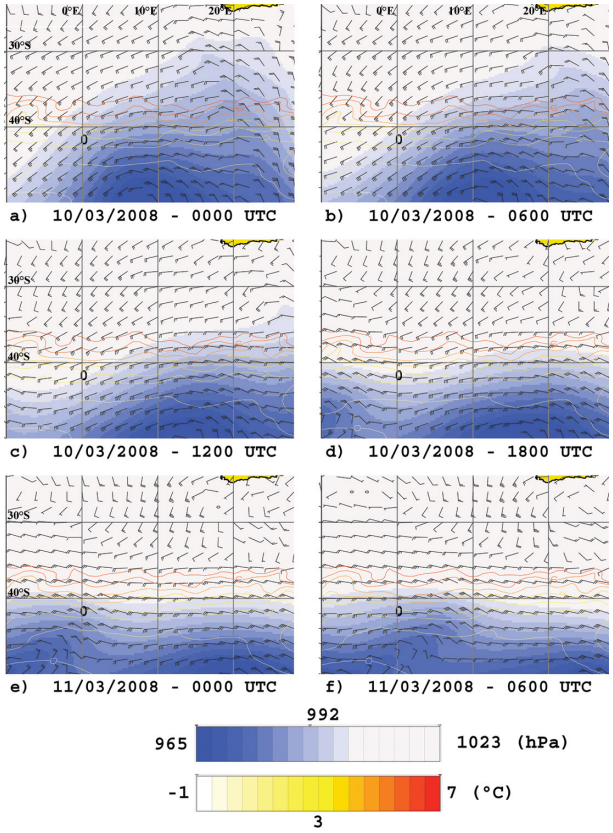

Fig. 10. Synoptic situation during the 10 and 11 March (from ECMWF ERA interim reanalysis). Colored background is the medium sea level pressure, isolines are SST (contour interval is 1 °C). Wind barbs (in knots) are overlaid. "O" indicates the ship location (42.5° S/9° E).

OSD
9, 1387–1436, 2012

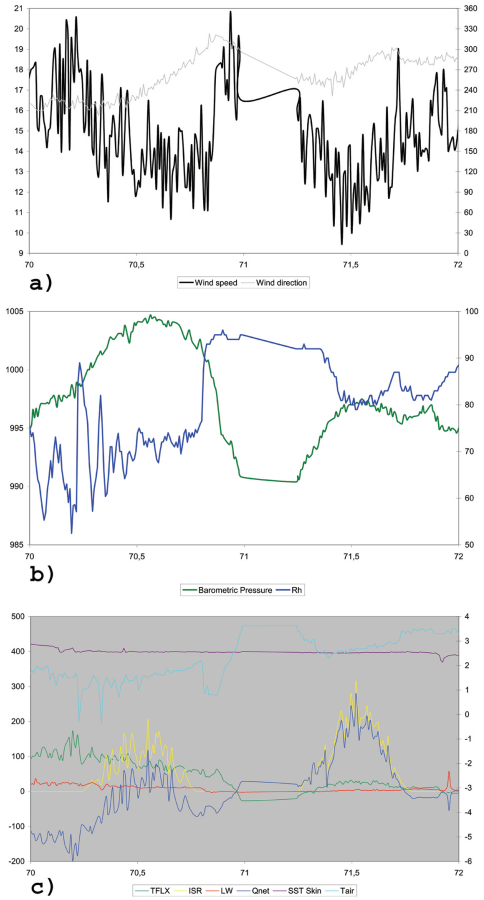

Fig. 11. Same as Fig. 7.

OSD
9, 1387–1436, 2012

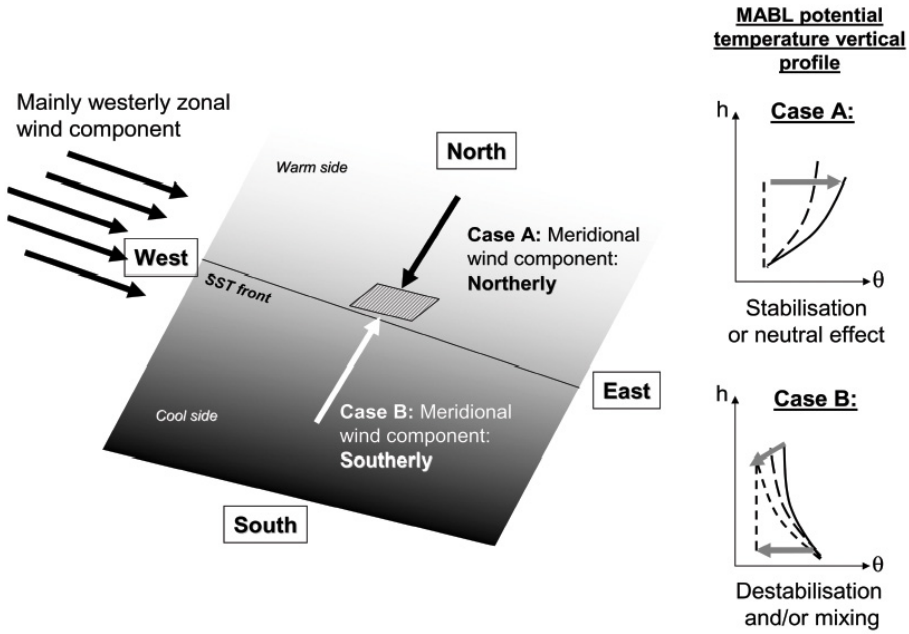

Fig. 12. A scheme of the wind effects driven by the atmospheric synoptic features. The wind variability affects the turbulent heat flux, the vertical shear and consequently the vertical stability of the MABL.

OSD
9, 1387–1436, 2012